ACS OMEGA

Open Access

This article is licensed under CC-BY-NC-ND 4.0

http://pubs.acs.org/journal/acsodf

Article

New Formulas for Evaluation of Cyclohexanol Solidification on Substrates with Surface Nanostructures

Yosuke Hanawa,* Jianliang Zhang, Agus P. Sasmito, Minghan Xu, Saad Akhtar, Mohammaderfan Mohit, Junichi Yoshida, Koichi Sawada, Yuta Sasaki, and Atsushi Sakuma

Cite This: *ACS Omega* 2024, 9, 24299−24307

Read Online

ACCESS | Metrics & More | Article Recommendations | Supporting Information

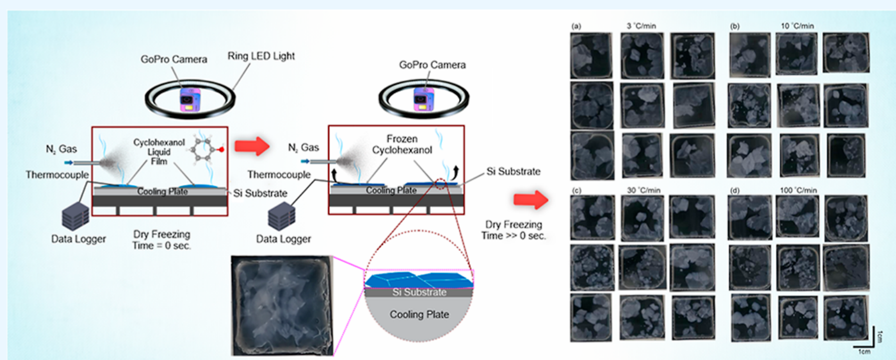

ABSTRACT: In semiconductor manufacturing, the sublimation drying process is crucial but poorly understood—particularly regarding the solidification of agents such as cyclohexanol on Si substrates. This knowledge gap results in inconsistent film properties and risks such as structural collapse. To address this critical gap in knowledge, the present study focused on an in-depth examination of the nucleation behavior exhibited by cyclohexanol during its cooling and solidification on Si substrates. Using a digital camera (GoPro10), the solidification process in experiments was recorded for a range of cooling rates and using substrates with distinct surface patterns. To evaluate temporal changes in crystal nucleation, video images were visually checked, and the temporal changes in the number of nuclei were examined. For a more quantitative analysis, the least-squares method was successfully employed to correlate mathematical equations to time-dependent nucleation data. Interestingly, the outcomes revealed significant correlations between the nucleation rate, cooling rate, and substrate pattern. In summary, this research offers a robust experimental framework for understanding the complex solidification behavior of cyclohexanol on Si substrates. The study contributes both qualitative and quantitative analyses, enriching our understanding of the variables that govern the solidification process, which has significant implications for enhancing the overall reliability and efficiency of semiconductor manufacturing.

■ INTRODUCTION

The shrinkage of semiconductor devices and the resulting integration of transistors have generally progressed in accordance with Moore's law.[1] Consequently, the performance and cost of semiconductor devices have rapidly increased, and the use of semiconductors in personal computers, smartphones, data centers, and other applications has become more widespread.[2]

With the extensive utilization of semiconductors, designing nanostructures with extraordinary electronic and optoelectronic properties has become increasingly important.[3] Specifically, vertical nanostructures with a high aspect ratio (HAR) exhibit higher surface energy or increased nanoparticle activity.[4] However, a primary obstacle in the production of these nanostructures is pattern collapse, which is a form of damage caused by capillary forces arising from various solution-based processes (also known as wet processes) employed during their fabrication.[5−7] These solution-based processes include wet etching,[8,9] hydrothermal synthesis,[10] and chemical bath deposition.[11]

An effective approach to address the pattern collapse of HAR nanostructures is sublimation drying.[12,13] This technique is often used for drying delicate materials, such as heat-sensitive pharmaceuticals or sensitive biological samples, where the direct application of heat may cause deformation or degradation of the materials.[14−16] The sublimation drying process comprises two steps: (1) the deposition of the sublimation agent/chemical on

Received: December 13, 2023
Revised: April 22, 2024
Accepted: May 16, 2024
Published: May 28, 2024

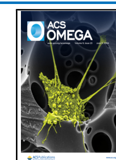

© 2024 The Authors. Published by American Chemical Society

the Si substrate through cooling solidification or precipitation solidification and (2) solid-phase sublimation drying accomplished by inert gas spraying. Pattern collapse occurs during the solidification process (i.e., the primary step) owing to the nonuniformity of film properties within the substrate surface.[17] Therefore, a comprehensive understanding of the solidification behavior of the sublimation chemical is vital for predicting the collapse of semiconductor nanostructures.

Solidification—the phase transition from liquid to solid—is an unfinished science that is not fully understood owing to its involvement in multiple scales and physical fields.[18] The process typically involves five stages: supercooling of the liquid, nucleation, recalescence, freezing, and subcooling of the solid.[19] In the context of solidification on Si substrates, the nucleation and recalescence stages are crucial; in the nucleation stage, the location of the first ice embryo is determined; and in the recalescence stage, the evolution of crystal growth can lead to the collapse of nanostructures.[17] Although considerable effort has been directed toward predicting nucleation and crystal growth, a key research gap that requires further investigation concerns the pattern collapse of HAR nanostructures depending on the size of Si substrates. The freezing behavior of water droplets on Si substrates has been investigated; however, previous studies focused on microdroplets on the Si substrate, and micropatterns were used rather than nanopatterns.[20−24] As solidification is a multiscale problem, the solidification behavior can vary among different scales. Another major gap is related to the geometry and type of sublimation chemicals. The preferable geometry for the sublimation chemical is a thin film, rather than droplets,[20−25] and most studies[25−27] have focused on materials that are not sublimation agents, such as water and hydroxyapatite. Consequently, the influence of sublimation-agent solidification on the Si substrate in relation to the collapse of nanostructures on the substrate is yet to be clarified. Thus, the mechanisms underlying the formation of uniform solidified films that inhibit collapse requirements remain unknown. In contrast to bulk materials, thin films undergo directional solidification, which necessitates appropriate equipment design.

Considering the aforementioned research gaps, the objective of this study was to broadly classify the nonuniform solidification process in sublimator thin films wetted over the entire surface of the Si substrate—particularly nucleation as a starting point for crystallization in the presence of disturbances such as vibration. Specifically, the nucleation behavior of cyclohexanol—an organic sublimation agent—during cooling and solidification on bare Si and patterned Si substrates is analyzed; the bare Si substrate was a Si substrate with a flat surface, whereas the patterned Si substrate had nanostructures on its surface. Cyclohexanol has a crystal form known as glass crystal[28] and is an organic compound with a melting point of 23 °C and vapor pressure of 0.13 kPa (at 20 °C) in the solid phase.[29,30] The freezing point of cyclohexanol is close to room temperature, making it an easier sublimation agent to handle than ice in semiconductor processes.

EXPERIMENTAL SECTION

Samples and Observation Methods. Figure 1 depicts the experimental apparatus employed in this study. Unlike previous studies,[20,21] two samples were prepared: one for observation of solidification dynamics and the other for temperature monitoring. This allowed us to verify that the actual temperature operation was in accordance with the settings (see the Supporting Information for actual temperature data). Cyclohexanol—the sublimation agent—was dispensed in 250 μL portions on each substrate so that the entire surface was wetted and spread, and it was then cooled by a Peltier device. One substrate's solidification process was recorded using a high-speed camera (GoPro Inc., GoPro Hero10:60 fps, 1080p), while the accompanying temperature fluctuations on the other substrate were recorded using a 0.1 mm K-type thermocouple to ensure that the experiment was performed at the prescribed cooling rate. The temperature data were logged at a frequency of 10 Hz using a Keyence NR-600 data logger. To facilitate ring illumination, an LDR2-170SW2-LA unit (CCS) was deployed. A modified CHP-77HI (Sensor Controls Co., Ltd., Japan) served as the Peltier device, which was regulated by an FC-3510 controller (Sensor Controls Co., Ltd., Japan).

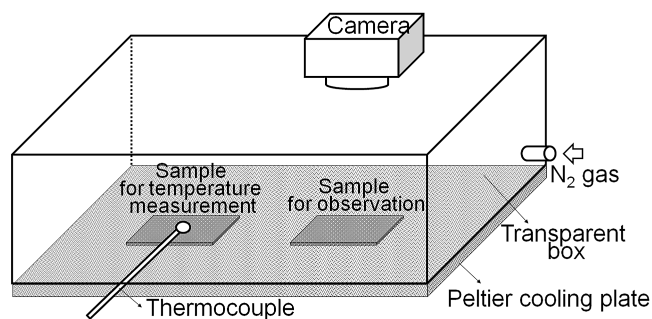

Figure 1. Schematic of the observation system utilizing two samples on a substrate, cooled via a Peltier element.

For the experiments, two types of substrates were employed. The first was a pristine bare Si substrate [P-type, B-doped (100) planes, with a resistivity range of 1−100 Ω cm], and the second was a coupon extracted from a patterned Si substrate.[31] The latter featured a square-layout Si cylinder pattern with the following approximate dimensions: a diameter of 30 nm, spacing of 60 nm, and height of 500 nm, covering an area of approximately 2 cm^2. Cyclohexanol sourced from FUJIFILM Wako Pure Chemical Corporation (Japan) with a purity of 98% was used as a special-grade reagent.

The observational procedure is detailed as follows.

1 UV treatment of the Si substrate for 20 min to remove organic matter.[32]
2 Application of 250 μL of cyclohexanol onto each substrate, equivalent to a 500 μm film thickness (the liquid film covers the entire coupon surface to avoid wetting effects).
3 Nitrogen inflow into the atmosphere control box at approximately 3 L/min.
4 Commencement of recording.
5 Activation of the light-emitting diode; concurrent initiation of temperature data logging for synchronization.
6Sequential Peltier temperature control:
   a Sustaining a temperature of 28 °C, exceeding the melting point of 23 °C, for 1 min.
   b Cooling to below the melting point at specified rates (3 °C with a holding time of 3 min).
   c Increasing the temperature to 28 °C at a rate of 100 °C/min for remelting the sublimation agent.
7 Termination of recording.

Employing these parameters and procedures, the solidification behavior of cyclohexanol was investigated at four distinct cooling rates—3, 10, 30, and 100 °C/min—on both bare and patterned Si substrates. Each cooling condition was

https://doi.org/10.1021/acsomega.3c09972
ACS Omega 2024, 9, 24299−24307

assessed 5−9 times to ensure the reliability of the results. The term "cooling rate" refers to the programmed setting of the cooling plate. All the experiments were performed in a class 30 (0.3 μm) FED-STD 209D clean room (temperature: 23 ± 1 °C, humidity: 50% ± 1%, external pressure difference: 30−50 Pa).

Crystal Counting Method. Subsequently, the captured videos were subjected to a meticulous temporal analysis to quantify the variations in the number of emerging crystal nuclei. Figure 2 illustrates the progression of crystal nuclei over a period

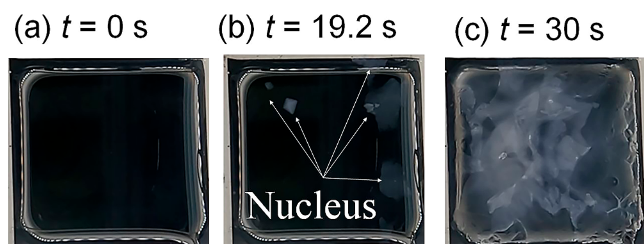

Figure 2. Enumeration of nucleation events captured visually.

of 30 s. Regions with nucleus formation exhibited a clouded appearance, as shown in Figure 2b. The differentiation in luminance levels substantially assisted the precise localization of crystal nucleus initiation. Both the timestamps and quantities of newly formed crystal nuclei were carefully documented. To obtain a visual representation of the temporal pattern, the aggregate number of generated crystals—hereinafter referred to as count I—was calculated at each specified time point and graphically represented. This facilitated the exploration of the temporal trends in crystal nucleation.

Evaluation Formulas. For a mathematical description of the temporal fluctuations in crystal nucleation events, two specific functions (I_A and I_W) were employed: eqs 1 and 2 are consistent with Arrhenius-type[33] and Weibull-type formulations,[34] respectively.

$$I_A(t) = A\exp\left(-\frac{B}{t - t_0}\right) \quad (1)$$

$$I_W(t) = \alpha\{1 - \exp\left(-\beta(t - t_0)\right)\} \quad (2)$$

Here, t denotes time, t_0 signifies the initial point of nucleation, and A, B, α, and β are constants. The equations were employed to fine-tune the constants A, B, α, and β using the least-squares method. The solver function in Microsoft Excel[35] was utilized to optimize these parameters, aiming to closely align the temporal variations in the aggregate nucleation count with the specific cooling rates and substrates under consideration.

RESULTS AND DISCUSSION

Solidification Observation. Figure 3 provides visual evidence of solidification on different coupons for the bare Si substrate, revealing that the number of crystal nuclei increased with the cooling rate. Figure 4 shows only the typical solidification images from Figure 3 for each cooling rate. Compared with Figure 3, this figure more clearly demonstrates that the number of nucleations increases at each cooling rate. Similarly, Figure 5 shows the solidification process on different

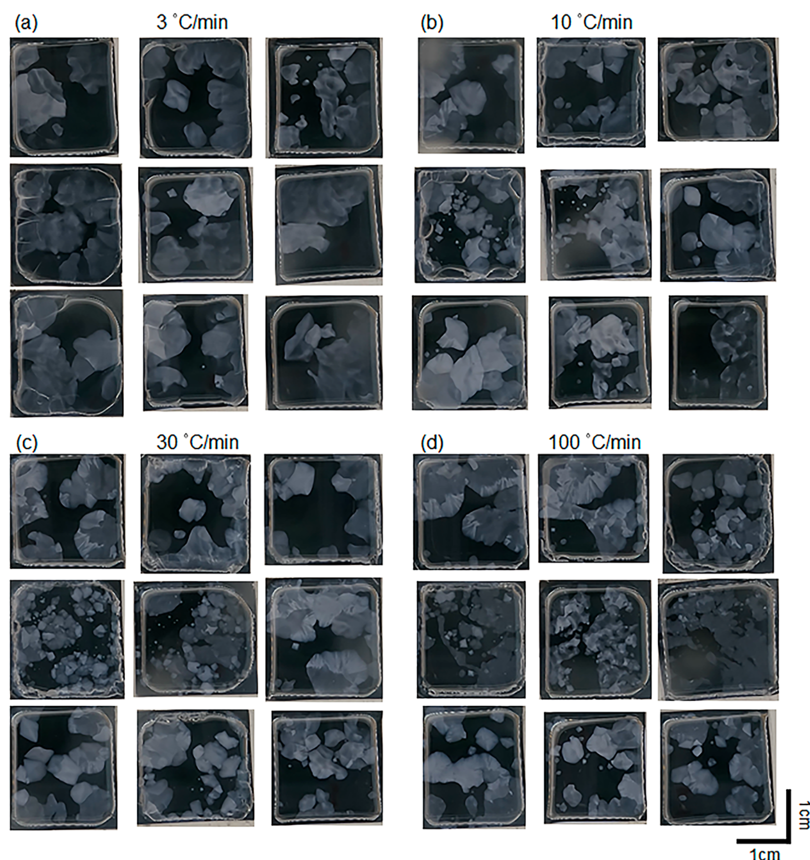

Figure 3. Morphological variations of cyclohexanol crystals due to the different Si coupons on a bare Si substrate at different cooling rates. (a−d) Correspond to cooling rates of 3, 10, 30, and 100 °C/min, respectively (Si coupon size was approximately 2 × 2.5 cm^2).

https://doi.org/10.1021/acsomega.3c09972
ACS Omega 2024, 9, 24299−24307

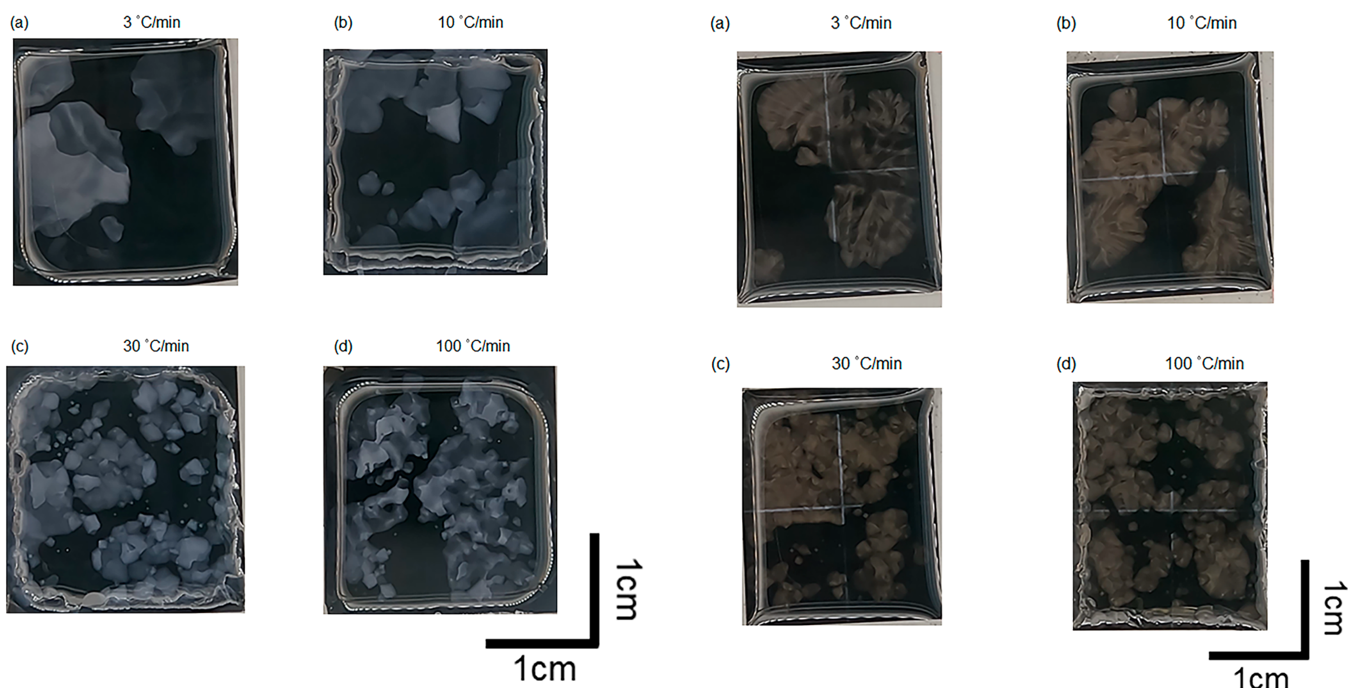

Figure 4. Typical morphological variations of cyclohexanol crystals on a bare Si substrate at different cooling rates. (a−d) Correspond to cooling rates of 3, 10, 30, and 100 °C/min, respectively (Si coupon size was approximately 2 × 2.5 cm^2).

Figure 6. Typical morphological variations of cyclohexanol crystals on a patterned Si substrate at different cooling rates. (a−d) Correspond to cooling rates of 3, 10, 30, and 100 °C/min, respectively (Si coupon size was approximately 2 × 2.5 cm^2).

coupons for the patterned Si substrate, and the number of crystal nuclei increases with the cooling rate. Figure 6 shows only the typical solidification images from Figure 5 for each cooling rate. Bubbles were not observed in any experiment in the cyclohexanol solidified film that was visually observed. The difference in the appearance of the cyclohexanol solids was assumed to be caused by the differences in the shape and crystal orientation of the solidified film. The nucleation points were random. The location of nucleation can be determined on the basis of the video recorded using this observation method. A more nuanced analysis of this phenomenon is presented in Figures 7 and 8, which depict time−series graphs that elucidate the total count of

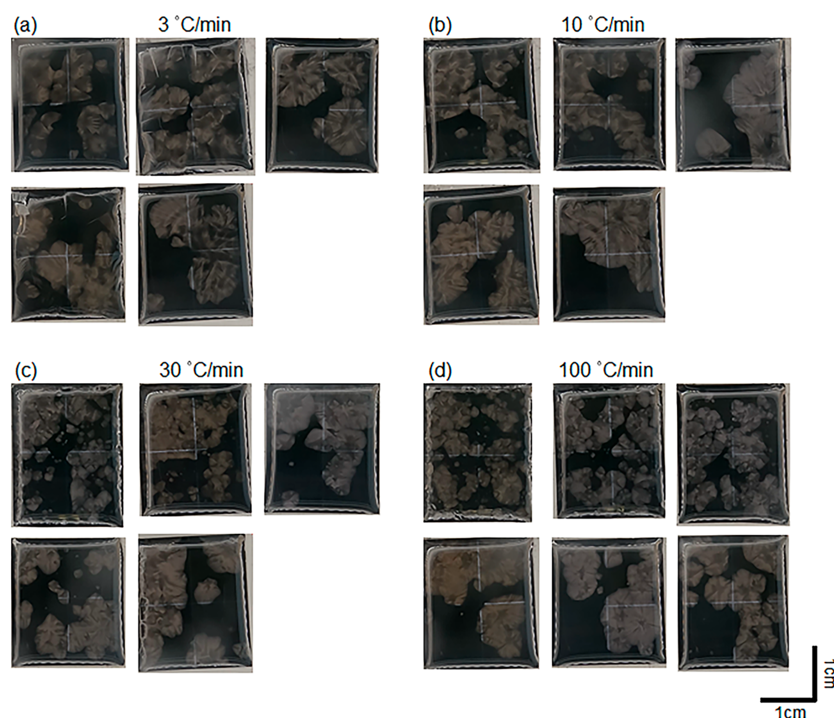

Figure 5. Morphological variations of cyclohexanol crystals due to the different Si coupons on a patterned Si substrate at different cooling rates. (a−d) Correspond to cooling rates of 3, 10, 30, and 100 °C/min, respectively (Si coupon size was approximately 2 × 2.5 cm^2).

https://doi.org/10.1021/acsomega.3c09972
ACS Omega 2024, 9, 24299−24307

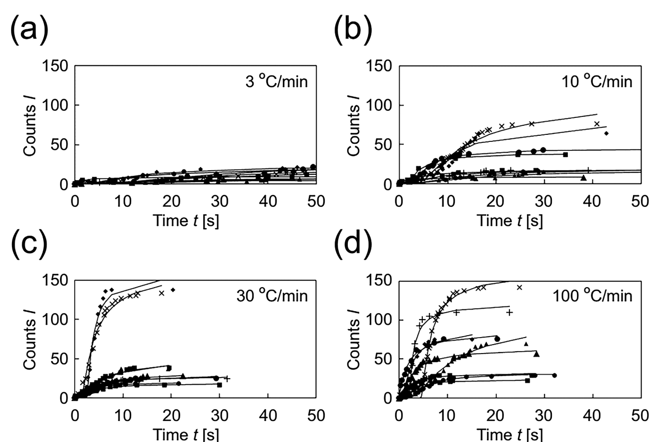

Figure 7. Plots of experimental values (indicated by dots) and fitted curves based on the Arrhenius-type equation (represented by lines) at different cooling rates for a bare Si substrate. (a−d) Results obtained cooling rates of 3, 10, 30, and 100 °C/min, respectively.

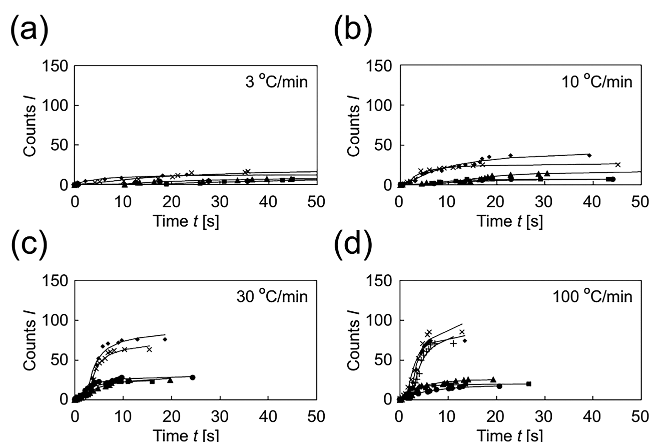

Figure 8. Plots of experimental values (indicated by dots) and fitted curves based on the Arrhenius-type equation (represented by lines) at different cooling rates for a patterned Si substrates. (a−d) Results at cooling rates of 3, 10, 30, and 100 °C/min, respectively.

visually identified crystal nuclei (referred to as I) and feature fitted lines based on the Arrhenius-type formula denoted by eq 1 for each solidification process. These graphs provide quantitative insights into the variation in the number of crystal nuclei at different cooling rates. It should be noted that the actual number of crystal nuclei fluctuated considerably depending on the value of N used in the experiments. This observation aligns with the findings of Yue et al.,[21] who reported a longer time necessary for droplet freezing initiation (i.e., fewer crystal nuclei formed) in patterned substrates.

Figures 7 and 6 additionally present the outcomes of fitting the observed data to the total count of crystal nuclei on both bare Si and patterned Si substrates. Eq 1 was employed for this purpose. The empirical values are denoted by discrete points, while the fitted lines correspond to the values computed through eq 1. Figure 7a−d pertain to bare Si substrates, and Figure 8a−d pertain to patterned Si substrates. In both scenarios, the experimental and calculation results agreed well.

Figure 9 shows the mean value (count $\overline{I}$) and the coefficient of variation (CV) for the total number of nuclei generated on each substrate type at different cooling rates.

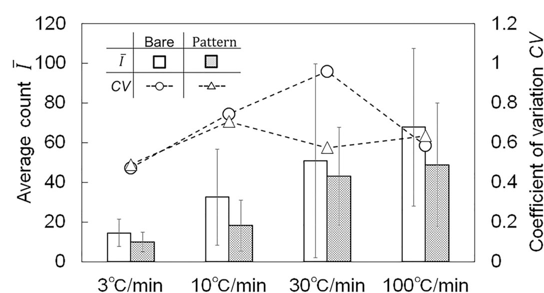

Figure 9. Mean quantity of nucleation events and corresponding CV with respect to the cooling rate and substrate type.

$$\mathrm{CV} = \frac{\sigma}{\overline{I}} \tag{3}$$

Here, σ represents the standard deviation of the number of generated crystal nuclei for each experimental condition. As shown in Figure 9, a reduction in the cooling rate was correlated with a decline in the generation of nuclei. Moreover, bare Si substrates manifested a higher overall nucleus count than the patterned Si substrates, along with larger differences in the CV among different cooling rates. The trend shown in Figure 9 suggests that any further increment in the cooling rate is unlikely to introduce significant perturbations in the CV, for both the bare and patterned Si substrates.

Evaluation Using Arrhenius-Type Formula. Figure 10 presents the mean values of fitting parameters A and B from eq 1

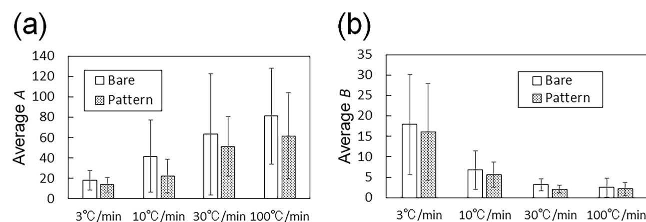

Figure 10. Mean values of parameters A (a) and B (b) for each cooling rate and substrate. These parameters from eq 1 have been adjusted to align with experimental findings.

for each substrate type at different cooling rates. The value of A exhibited a direct relationship with the cooling rate and was consistently larger for bare Si substrates than that for patterned Si substrates. Conversely, B decreased as the cooling rate increased, and the difference between the two types of substrates was not as pronounced as that for A.

Figure 11 depicts the results of exponential, progressive, and logarithmic approximations, relative to the cooling-rate dependence of mean values A and B. Excellent agreement between experimental values and these approximations was observed—particularly for the progressive and logarithmic approximations of A—for both bare and patterned Si substrates. Table 1 presents the approximate formulas alongside their respective coefficients of determination (R^2) for each approximation type.

A comparative analysis between progressive and logarithmic approximations for A revealed a substantial difference in behavior at cooling rates below 10 °C/min. The logarithmic approximation exhibited a precipitous decline below this threshold, approaching zero at 1 °C/min. This phenomenon was accentuated in the case of the patterned Si substrate. In contrast, the progressive approximation exhibited an asymptotic decrease. According to eq 1, A = 0 at 1 °C/min implies the

https://doi.org/10.1021/acsomega.3c09972
ACS Omega 2024, 9, 24299−24307

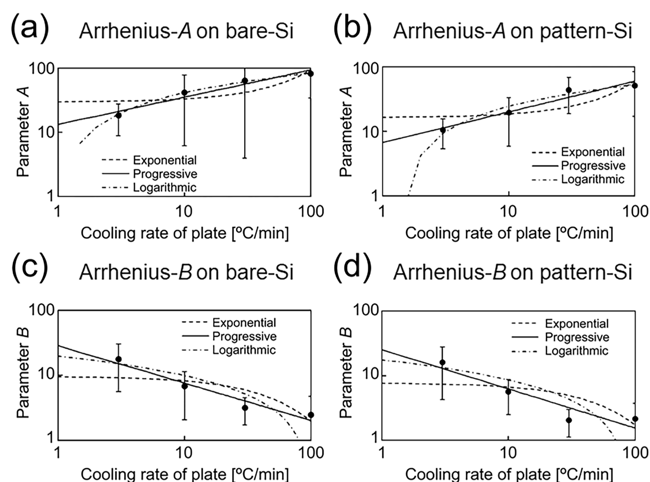

Figure 11. Exponential, progressive, and logarithmic models approximating the cooling-dependent behavior of parameters A and B in eq 1. (a,b) Approximations for parameter A on bare Si and patterned Si substrates, respectively. (c,d) Approximations for parameter B on bare Si and patterned Si substrates, respectively.

Table 1. Approximations of Coefficients A and B in eq 1 and the Coefficients of Determination (R^2)

		bare	patterned
A	exponential	$y = 29.5e^{0.0115x}$, $R^2 = 0.600$	$y = 19.8e^{0.013x}$, $R^2 = 0.658$
	progressive	$\mathbf{y = 13.3x^{0.423}}$, $\mathbf{R^2 = 0.934}$	$\mathbf{y = 8.50x^{0.4585}}$, $\mathbf{R^2 = 0.945}$
	logarithmic	$y = 18.1 \ln(x) - 0.566$, $R^2 = 0.996$	$y = 14.8 \ln(x) - 4.96$, $R^2 = 0.943$
B	exponential	$y = 9.67e^{-0.016x}$, $R^2 = 0.601$	$y = 7.75e^{-0.015x}$, $R^2 = 0.493$
	progressive	$\mathbf{y = 28.6x^{-0.575}}$, $\mathbf{R^2 = 0.939}$	$\mathbf{y = 25.1x^{-0.605}}$, $\mathbf{R^2 = 0.874}$
	logarithmic	$y = -4.29 \ln(x) + 19.8$, $R^2 = 0.816$	$y = -3.91 \ln(x) + 17.6$, $R^2 = 0.787$

absence of crystal nuclei formation. However, our experimental data indicated crystal nucleation even at this low cooling rate, contradicting the implications of the logarithmic approximation. In contrast, the progressive approximation derived from eq 1 yields a nonzero value for A at 1 °C/min, corroborating the experimental evidence of crystal nucleation. Thus, the progressive approximation is a more accurate mathematical representation, closely mirroring our empirical findings. Both A and B values are accurately encapsulated by this approximation.

A comparative examination of the progressive approximation for A between bare and patterned Si substrates revealed that the coefficient preceding the cooling-rate variable (x) is substantially larger for the bare Si substrate. In contrast, minimal fluctuation is observed in the exponent of the rate variable (x). This suggests a near-constant ratio of A values between the bare and patterned Si substrates, regardless of the cooling rate x. Conversely, for B, both the coefficient preceding x and the exponent of x exhibited minimal deviation between the bare and patterned Si substrates. This implies that the value of B remains relatively invariant for the two substrate types.

Evaluation Using Weibull-Type Formula. Figures 12 and 13 present the results of fitting the empirical data concerning the total number of crystal nuclei on bare and patterned Si substrates to eq 2. This equation provides a probability theory for continuous probability distributions that can model random variables, the time between events, etc., whereas eq 1 is a formula for the temperature dependence of reaction rates. In the figures, the dots symbolize the experimental findings, whereas the lines

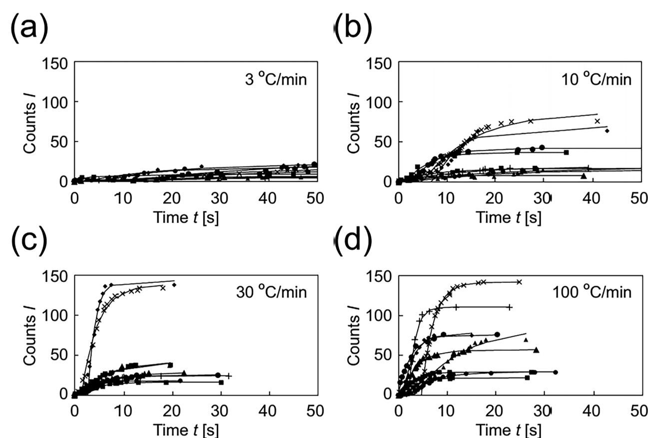

Figure 12. Experimental values (dots) of the count I and fitting based on the Weibull-type equation (line) at different cooling rates for bare Si: (a−d) results at cooling rates of 3, 10, 30, and 100 °C/min, respectively.

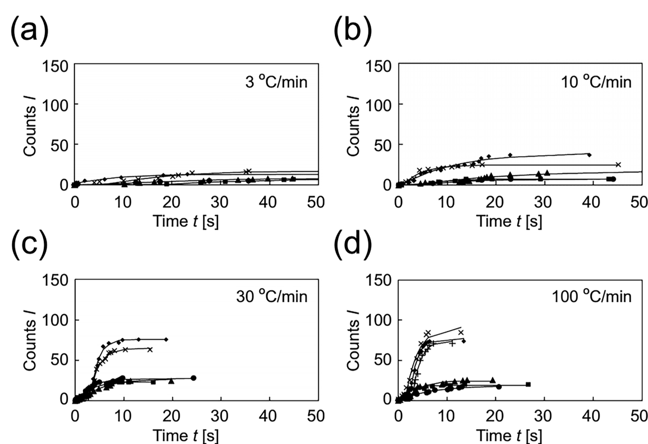

Figure 13. Experimental values (dots) of the count I and fitting curves based on the Weibull-type equation (lines) at different cooling rates for patterned Si: (a−d) results at cooling rates of 3, 10, 30, and 100 °C/min, respectively.

signify the values extrapolated using eq 2. Figure 12a−d presents the outcomes for bare Si, and Figure 13a−d presents the results for patterned Si. For both substrate types, the experimental and calculated values agreed well.

Figure 14 presents the mean values of α and β for each cooling rate and substrate type. As shown, α increased with the cooling rate, in agreement with eq 1. Moreover, α consistently reached larger values for the bare Si substrate than that for the patterned Si substrate. β also increased with the cooling rate; however, compared to α, patterned Si exhibited higher β values than bare Si, thereby diverging from the implications of eq 1. Figure 15

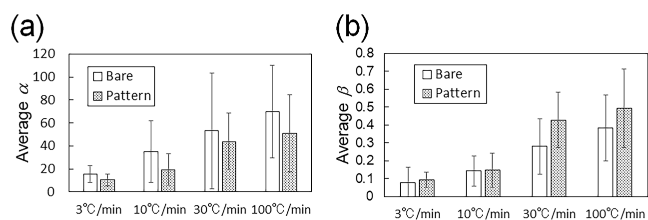

Figure 14. Mean values of parameters α (a) and β (b) for each cooling rate and substrate type. These parameters from eq 2 have been adjusted to correspond to the experimental values.

https://doi.org/10.1021/acsomega.3c09972
ACS Omega 2024, 9, 24299−24307

presents the outcomes of exponential, progressive, and logarithmic approximations applied to determine the cooling-rate dependence of α and β.

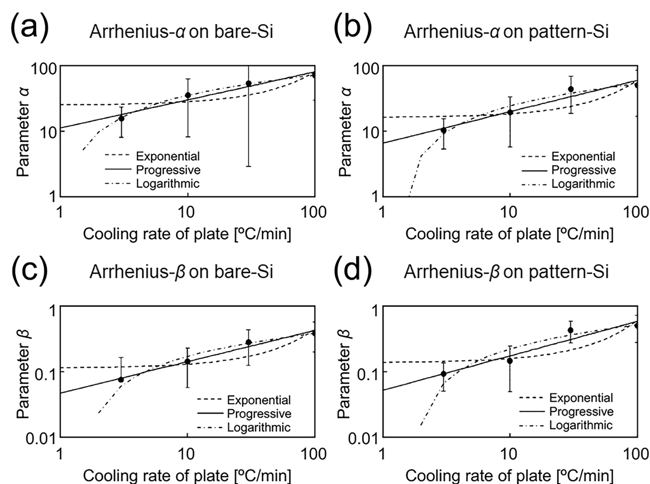

Figure 15. Exponential, progressive, and logarithmic models approximating the cooling-dependent behavior of parameters α and β in eq 2. (a,b) Approximations for parameter α on bare Si and patterned Si substrates, respectively. (c,d) Approximations for parameter β on bare Si and patterned Si substrates, respectively.

As illustrated in the figures, the experimental data agreed well with both the progressive and logarithmic approximations for parameters α and β, regardless of the substrate type (bare or patterned Si). Table 2 presents each approximation method along with the corresponding coefficient of determination (R^2). Notably, although the logarithmic approximation attained a higher R^2 value, it predicts the implausible cessation of crystal nucleation as the cooling rate approaches 1 °C/min. Thus, the progressive approximation based on eq 1 more accurately represents empirical observations.

An evaluation of the progressive approximation for α between bare Si and patterned Si substrates revealed that the coefficient preceding the cooling-rate variable x was larger for bare Si. However, the exponent x remained relatively stable. This indicated that the ratio of α values between bare Si and patterned Si remained relatively constant, mirroring the behavior given by eq 1. Analogously, for β, neither the coefficient nor the exponent of x exhibited appreciable disparities between the two substrate types. Consequently, the β values for bare Si and patterned Si were remarkably consistent, aligning well with eq 1.

For the progressive approximations derived from eqs 1 and 2, the values of both A and α were similar between bare Si and patterned Si. A comparison between the coefficients of determination for the progressive approximation for Arrhenius- and Weibull-type formulas indicated that the latter generally yields larger R^2 values. This is attributed to the dynamic nature of crystal nucleation over time, for which the Weibull-type formula offers a more nuanced fit. However, the applicability of this formula at extremely low (≤1 °C/min) or high (≥100 °C/min) cooling rates remains to be empirically verified in future studies. The analysis of both equations suggests that the number of nucleations on patterned Si is smaller than that on bare Si between 1 and 100 °C/min. This may be due to the different freezing points of cyclohexanol on the substrates. It is known that the freezing point of organic chemicals decreases in the nanosized fine region.[31] This may be why the degree of undercooling of cyclohexanol on patterned Si was smaller than that on bare Si under the same cooling conditions, which may have suppressed the nucleation. These hypotheses can be tested in future research. While this study provides valuable insights, several limitations exist because the empirical equations is adopted, and other materials need to determine their variables individually. Additionally, more equations can be derived to describe some facets of the solidification process, such as the growth rates at the solid−liquid interface or temporal changes in the overall solidification area. Subsequent research will focus on extending this mathematical framework to accommodate other materials and additional aspects of the solidification process, including the rates of solid−liquid interface growth and the temporal dynamics of solidification areas.

■ CONCLUSIONS

In this study, an experimental apparatus was designed to investigate the solidification dynamics of cyclohexanol on Si substrates. Through modulation of both the substrate type and the cooling rate, the system facilitates real-time observations of the crystallization process. Temporal variations in the number of nucleated crystals in cyclohexanol were quantitatively analyzed, revealing dependence on both the cooling rate and the substrate. To assess these time-dependent changes in crystal nucleation, two mathematical models based on the Arrhenius and Weibull functions were developed. These models adequately captured the empirical data on the temporal progression of crystal nucleation, with the Weibull function exhibiting superior correspondence. Furthermore, the parameters A, B, α, and β in these equations were found to be influenced by the cooling rate. A progressive approximation method was employed to derive coefficients for these evaluation equations, allowing the prediction of nucleation rates under diverse cooling conditions. The findings of this study can advance our understanding and computational modeling of two-dimensional solidification behavior in a variety of materials. This research has significant implications for fields such as thin-film fabrication, electro-deposition, and freeze-drying technologies.

Table 2. Approximations of Coefficients α and β as Given by eq 2, along with the Corresponding Coefficients of Determination (R^2)

		bare	patterned
α	exponential	$y = 24.9e^{0.0117x}$, $R^2 = 0.617$	$y = 16.2e^{0.0131x}$, $R^2 = 0.623$
	progressive	$\mathbf{y = 11.2x^{0.426}}$, $\mathbf{R^2 = 0.942}$	$\mathbf{y = 6.69x^{0.476}}$, $\mathbf{R^2 = 0.939}$
	logarithmic	$y = 15.6\ln(x) - 1.12$, $R^2 = 0.998$	$y = 12.5\ln(x) - 4.39$, $R^2 = 0.944$
β	exponential	$y = 0.113e^{0.0137x}$, $R^2 = 0.699$	$y = 0.136e^{0.0148x}$, $R^2 = 0.642$
	progressive	$\mathbf{y = 0.0473x^{0.477}}$, $\mathbf{R^2 = 0.976}$	$\mathbf{y = 0.0522x^{0.522}}$, $\mathbf{R^2 = 0.920}$
	logarithmic	$y = 0.0912\ln(x) - 0.0397$, $R^2 = 0.980$	$y = 0.127\ln(x) - 0.0725$, $R^2 = 0.908$

https://doi.org/10.1021/acsomega.3c09972
ACS Omega 2024, 9, 24299−24307

■ ASSOCIATED CONTENT

Supporting Information

The Supporting Information is available free of charge at https://pubs.acs.org/doi/10.1021/acsomega.3c09972.

Time variation of the cyclohexanol temperature on bare Si or patterned Si samples for temperature measurement with a K-type thermocouple (PDF)

Solidification behavior of cyclohexanol at 3 and 100 °C/min on bare Si and patterned Si substrates (MP4)

■ AUTHOR INFORMATION

Corresponding Author

Yosuke Hanawa − *SCREEN Holdings Co., Ltd., Kyoto 612-8486, Japan;* orcid.org/0000-0001-9964-4794; Email: hanawa@screen.co.jp

Authors

Jianliang Zhang − *Faculty of Fiber Science and Engineering, Kyoto Institute of Technology, Kyoto 606-8585, Japan*

Agus P. Sasmito − *Department of Mining and Materials Engineering, McGill University, Montreal, Quebec H3A 0E8, Canada;* orcid.org/0000-0003-3444-8922

Minghan Xu − *Department of Mining and Materials Engineering, McGill University, Montreal, Quebec H3A 0E8, Canada*

Saad Akhtar − *GERAD and Department of Mathematics and Industrial Engineering, Polytechnique Montreal, Montreal, Quebec H3T 1N8, Canada*

Mohammaderfan Mohit − *Department of Mining and Materials Engineering, McGill University, Montreal, Quebec H3A 0E8, Canada*

Junichi Yoshida − *SCREEN Holdings Co., Ltd., Kyoto 612-8486, Japan*

Koichi Sawada − *SCREEN Holdings Co., Ltd., Kyoto 612-8486, Japan*

Yuta Sasaki − *SCREEN Holdings Co., Ltd., Kyoto 612-8486, Japan;* orcid.org/0000-0002-4576-3103

Atsushi Sakuma − *Faculty of Fiber Science and Engineering, Kyoto Institute of Technology, Kyoto 606-8585, Japan*

Complete contact information is available at: https://pubs.acs.org/10.1021/acsomega.3c09972

Author Contributions

All authors participated in conceptualizing and designing the study. Hanawa and Xu were responsible for material preparation and data acquisition. The numerical computations were undertaken by Hanawa, Zhang, and Sakuma. The manuscript's initial draft was authored by Hanawa, and each author provided constructive feedback on previous versions of the manuscript.

Funding

This research was financially supported by SCREEN Holdings Co., Ltd. In addition, Atsushi Sakuma received an Academic Guidance Grant from SCREEN Holdings Co., Ltd.

Notes

The authors declare the following competing financial interest(s): This research was financially supported by SCREEN Holdings Co., Ltd. In addition, Atsushi Sakuma received an Academic Guidance Grant from SCREEN Holdings Co., Ltd.

■ ACKNOWLEDGMENTS

We thank the members of SCREEN Semiconductor Solutions, Inc., for their fruitful discussions and for reviewing the manuscript. We also thank Editage (www.editage.com) for the English-language editing.

■ ABBREVIATIONS

CV, coefficient of variation; HAR, high aspect ratio; LED, light-emitting diode

■ REFERENCES

(1) Moore, G. E. Cramming More Components Onto Integrated Circuits. *Proc. IEEE* **1998**, *86*, 82−85.

(2) Waldrop, M. M. The chips are down for Moore's law. *Nature* **2016**, *530*, 144−147.

(3) Böer, K. W.; Pohl, U. W. *Semiconductor Physics*; Springer Nature: Germany, 2023.

(4) Ghosh, T.; Fritz, E. C.; Balakrishnan, D.; Zhang, Z.; Vrancken, N.; Anand, U.; Zhang, H.; Loh, N. D.; Xu, X.; Holsteyns, F.; Nijhuis, C. A.; Mirsaidov, U. Preventing the capillary-induced collapse of vertical nanostructures. *ACS Appl. Mater. Interfaces* **2022**, *14*, 5537−5544.

(5) Chini, S. F.; Amirfazli, A. Understanding pattern collapse in photolithography process due to capillary forces. *Langmuir* **2010**, *26*, 13707−13714.

(6) Sasaki, Y.; Yamazaki, T.; Kimura, Y. Liquid-cell transmission electron microscopy observation of two-step collapse dynamics of silicon nanopillars on evaporation of Propan-2-ol: implications for semiconductor integration density. *ACS Appl. Nano Mater.* **2022**, *5*, 9495−9502.

(7) Jincao, Y.; Matthews, M. A.; Darvin, C. H. Prevention of photoresist pattern collapse by using liquid carbon dioxide. *Ind. Eng. Chem. Res.* **2001**, *40*, 5858−5860.

(8) Wang, L.; Zhu, Y.; Wen, R. T.; Xia, G. Sub-10 μm-thick Ge thin film fabrication from bulk-Ge substrates via a wet etching method. *ACS Omega* **2023**, *8* (51), 49201−49210.

(9) Choi, K.; Song, Y.; Ki, B.; Oh, J. Nonlinear etch rate of Au-assisted chemical etching of silicon. *ACS Omega* **2017**, *2* (5), 2100−2105.

(10) Balderas, R. I.; Ciobanu, C. V.; Richards, R. M. (111) Faceted Metal Oxides: A Review of Synthetic Methods. *Cryst. Growth Des.* **2022**, *22*, 6296−6322.

(11) Gupta, I.; Mohanty, B. C. Dynamics of surface evolution in semiconductor thin films grown from a chemical bath. *Sci. Rep.* **2016**, *6*, 33136.

(12) Patel, M. N.; Sirard, S.; Limary, R.; Hymes, D. Freeze drying of high aspect ratio structures. *Solid State Phenom.* **2014**, *219*, 119−122.

(13) Chen, H. W.; Verhaverbeke, S.; Gouk, R.; Leschkies, K.; Sun, S.; Bekiaris, N.; Visser, R. J. (Invited) Supercritical Drying: A sustainable solution to pattern collapse of high-aspect-ratio and low-mechanical-strength device structures. *ECS Trans.* **2015**, *69*, 119−130.

(14) Cho, J. H.; Gao, Y.; Ryu, J.; Choi, S. Portable, Disposable, paper-based microbial fuel cell sensor utilizing freeze-dried bacteria for in situ water quality monitoring. *ACS Omega* **2020**, *5* (23), 13940−13947.

(15) Capozzi, L. C.; Trout, B. L.; Pisano, R. From batch to continuous: freeze-drying of suspended vials for pharmaceuticals in unit-doses. *Ind. Eng. Chem. Res.* **2019**, *58*, 1635−1649.

(16) Lu, J.; Peng, W.; Lv, Y.; Jiang, Y.; Xu, B.; Zhang, W.; Zhou, J.; Dong, W.; Xin, F.; Jiang, M. Application of cell immobilization technology in microbial cocultivation systems for biochemicals production. *Ind. Eng. Chem. Res.* **2020**, *59*, 17026−17034.

(17) Sasaki, Y.; Hanawa, Y.; Otsuji, M.; Fujiwara, N.; Kato, M.; Yamaguchi, Y.; Takahashi, H. Breakthrough of sublimation drying by liquid phase deposition. *Solid State Phenom.* **2021**, *314*, 172−177.

(18) Ma, M.; Wang, Y.; Cao, X.; Lu, W.; Guo, Y. Temperature and supersaturation as key parameters controlling the spontaneous precipitation of calcium carbonate with distinct physicochemical properties from pure aqueous solutions. *Cryst. Growth Des.* **2019**, *19*, 6972−6988.

(19) Akhtar, S.; Xu, M.; Sasmito, A. P. Development and validation of a semi-analytical framework for droplet freezing with heterogeneous nucleation and non-linear interface kinetics. *Int. J. Heat Mass Transfer* **2021**, *166*, 120734.
(20) Qin, S.; Jin, Y.; Yin, F.; Wang, Z.; Bai, G. Can solid surface energy be a predictor of ice nucleation ability? *Appl. Surf. Sci.* **2022**, *602*, 154193.
(21) Yue, X.; Liu, W.; Wang, Y. Freezing delay, frost accumulation and droplets condensation properties of micro- or hierarchically-structured silicon surfaces. *Int. J. Heat Mass Transfer* **2018**, *126*, 442−451.
(22) Mishchenko, L.; Hatton, B.; Bahadur, V.; Taylor, J. A.; Krupenkin, T.; Aizenberg, J. Design of Ice-Free Nanostructured Surfaces based on Repulsion of Impacting water Droplets. *ACS Nano* **2010**, *4*, 7699−7707.
(23) Song, M.; Dang, C.; Higashi, T.; Hihara, E. Review of experimental data associated with the solidification characteristics of water droplets on a cold plate surface at the early frosting stage. *Energy Build.* **2020**, *223*, 110103.
(24) Tiwari, A.; Samanta, R.; Chattopadhyay, H. Droplet solidification: physics and modelling. *Appl. Therm. Eng.* **2023**, *228*, 120515.
(25) Akhtar, S.; Xu, M.; Sasmito, A. P. A novel crystal growth model with nonlinear interface kinetics and curvature effects: sensitivity analysis and optimization. *Cryst. Growth Des.* **2021**, *21*, 3251−3265.
(26) Lopatin, C. M.; Pizziconi, V. B.; Alford, T. L. Crystallization Kinetics of sol-gel derived hydroxyapatite Thin Films. *J. Mater. Sci.: Mater. Med.* **2001**, *12*, 767−773.
(27) Xu, M.; Hanawa, Y.; Akhtar, S.; Sakuma, A.; Zhang, J.; Yoshida, J.; Sanada, M.; Sasaki, Y.; Sasmito, A. P. Multi-scale analysis for solidification of phase change materials (PCMs): experiments and modeling. *Int. J. Heat Mass Transfer* **2023**, *212*, 124182.
(28) Adachi, K.; Suga, H.; Seki, S. Phase changes in crystalline and glassy-crystalline cyclohexanol. *Bull. Chem. Soc. Jpn.* **1968**, *41*, 1073−1087.
(29) Musse, M. T. *Ullmann's Encyclopedia of Industrial Chemistry*, 7th ed.; Wiley: New York, 2008.
(30) ILO and WHO. *ILO and WHO International Chemical Safety Card*, 2021; Vol. *0243*. https://www.ilo.org/dyn/icsc/showcard.display?p_card_id=0243&p_edit=&p_version=2&p_lang=en.
(31) Hanawa, Y.; Sasaki, Y.; Uchida, S.; Funayoshi, T.; Otsuji, M.; Takahashi, H.; Sakuma, A. Thermomechanical formulation of freezing point depression behavior of liquid on solid surface with nanostructure. *Proceedings of the ASME 2020 International Mechanical Engineering Congress and Exposition, Heat Transfer and Thermal Engineering; Virtual, Online*; ASME, 2020; Vol. *11*. Paper no. IMECE2020−23759.
(32) Weber, D.; Heimburger, R.; Schondelmaier, G.; Junghans, T.; Zetzl, A.; Zahn, D. R. T.; Schondelmaier, D. Cost-effective equipment for surface pre-treatment for cleaning and excitation of substrates in semiconductor technology. *SN Appl. Sci.* **2023**, *5*, 21.
(33) Peleg, M.; Normand, M. D.; Corradini, M. G. The Arrhenius equation revisited. *Crit. Rev. Food Sci. Nutr.* **2012**, *52*, 830−851.
(34) Weibull, W. A statistical distribution function of wide applicability. *J. Appl. Mech.* **1951**, *18*, 293−297.
(35) Harris, D. C. Nonlinear least-squares curve fitting with Microsoft Excel solver. *J. Chem. Educ.* **1998**, *75*, 119.

https://doi.org/10.1021/acsomega.3c09972
ACS Omega 2024, 9, 24299−24307